Received: 30 October 2025 | Revised: 30 January 2026 | Accepted: 19 May 2026 | Published online: 9 June 2026

RESEARCH ARTICLE

Journal of Optics and Photonics Research
2026, Vol. 00(00) 1–9
DOI: 10.47852/bonviewJOPR62028031

BON VIEW PUBLISHING

Tunable Phase Shifters for 6G Beamforming Networks

Victor Chepkech Naibei[1,*], Dismas Choge[1], James Jena[2], David Waswa[2] and Duncan Kiboi Boiyo[3]

[1] *Physics Department, University of Eldoret, Kenya*

[2] *Centre for Broadband Communication, Nelson Mandela University, South Africa*

[3] *Physics Department, Moi University, Kenya*

Abstract: The deployment of 6G network requires multiple number of antennas at the base station with multiple signals that undergo constructive interference to create thinner beams with more energy so as to mitigate path loss. This will support higher data rates, lower latency levels, and improved energy efficiency. This paper proposes a phase-shifting technology for beamforming that focuses radio energy to a specific user equipment, thus maximizing spectral efficiency. We present a novel approach of phase-shifting technology by generating tunable microwave pulses using the slicing-level technique in an optoelectronic oscillator (OEO) setup. Two laser sources undergo intensity and phase modulation using a well-characterized Mach–Zehnder modulator and a phase modulator. Modulating signals in the range of 100 kHz–13.3 MHz are used to generate microwave waveforms. Repetition-rate-tunable pulses are generated from the microwave waveforms using the slicing-level technique. Photonic-assisted tunable pulses generated have a pulse width ranging from 0.6 ns to 7.5 μs and a duty cycle ranging from 17% to 96% optimized for phase shifting (φ) of signals, with potential for multiple antenna elements, which act as time delays aimed at creating constructive interference of the beams that form a concentrated beam of energy. This work successfully creates phase shifters ranging from 14° to 299° that can be used to steer antennas for 6G network by controlling pointing angles at the antenna array terminals, which creates a multiplex transmission line as a linear combination of signals.

Keywords: phase shifting, antennas for 6G network, tunable microwave pulses

1. Introduction

The evolution of network generations is being necessitated by the desire to have a network that supports higher data rates, lower latency levels, and improved energy efficiency to address the large traffic of devices and the internet globally [1, 2]. 6G network will operate on higher frequency ranges above 95 GHz, and at this higher frequency, signals can encounter propagation challenges such as path loss, thus requiring essential beamforming techniques to focus the beam more narrowly to a specific target [3]. Efficiency of the spectrum is key, which aims at minimizing interference and energy loss during propagation; beamforming focuses radio energy to a specific required direction instead of sending it to all directions, thus maximizing spectral efficiency while concentrating beam energy to a specific user equipment (UE) [4]. Furthermore, the formation of beams with Multiple Input Multiple Output technology that is being used in 5G network has complications in terms of antenna element design, interference, and power loss, which requires more advanced beamforming techniques that can concentrate beams so as to have more energy being focused to a specific direction [5, 6]. The high frequencies of operation in communication face many challenges such as energy loss and interference arising from bad weather conditions such as heavy rain; these challenges can be overcome by utilizing multiple antenna elements whose signals are concentrated into one strong beam between base stations (BS) and users [7].

Beamforming aims at aligning and focusing signals from BS to UE, where the received signal can be used to determine the strength of the beam and the strongest beam can be reported back to BS [8]. The use of beamforming technology and alignment of antenna elements using a phase-array approach to focus beams to a specific required direction allows the energy of mmWave signals to be focused and transmitted over a long distance to users [9]. Tracking of the beams can be established by updating the beam orientations and widths of the beams along the trajectory. Beamforming orientations allow proper alignment between BS and UE for ample gain by minimizing interference [10, 11]. Phase-array technology can be used to control multiple interferences, especially when aiming at complex patterns [12]. Antennas are key in wireless communication; therefore, proper antenna alignment creates maximum spectral efficiency that successfully enhances beamforming to steer antennas for 6G network [13]. Phase shifting for steering antennas can be achieved by adjusting the duty cycle of microwave pulses.

Microwave waveforms can be used to generate photonic-assisted tunable microwave pulses. By adjusting direct current and the modulating frequency, the repetition rate of the pulses can be

***Corresponding author:** Victor Chepkech Naibei, Physics Department, University of Eldoret, Kenya. Email: ssciphym00321@uoeld.ac.ke

© The Author(s) 2026. Published by BON VIEW PUBLISHING PTE. LTD. This is an open access article under the CC BY License (https://creativecommons.org/licenses/by/4.0/).

varied [14]. While other published work records pulse durations of 24 ns and up to 165 ns, microwave pulses can be made tunable by adjusting the pulse width and period between adjacent pulses, which in turn affects the duty cycle [15, 16]. Tunable microwave pulses have the advantage of adjustable frequencies and a controllable duty cycle [17]. Beamforming techniques are aimed at improving the efficiency of the spectrum by minimizing power loss, ensuring low driving voltage, and focusing the beam more narrowly on the users [18]. Each square or sine wave has one photonic-assisted tunable pulse, with a duration that corresponds to the pulse repetition [19]. Periodic tunable pulses with short pulse width and period within the picoseconds, nanoseconds, and microseconds range are a candidate for improving sensitivity and range of resolutions [20, 21]. By tuning the modulating frequency of the scheme being used, the repetition rate and the duty cycle of the microwave-tunable pulses can be varied accordingly [22]. This work successfully creates phase shifting for phase-array antennas by adjusting the duty cycle of tunable microwave pulses. Increasing the number of antennas leads to a narrower beam with higher gain, making it more precise. This should however incorporate hybrid beamforming to minimize power consumption.

2. Principle of Operation

The experiment uses intensity and phase modulation to generate microwave signals and the slicing-level (SL) technique to generate photonic-assisted tunable pulses. Herein, the concept of the sum and difference frequencies was applied by optical heterodyning at the photodiode (PD). As a result, the beat frequency was equivalent to the difference in frequency of two interfering beats. The corresponding sine wave from the signal generator (SG) is represented by the following equation:

$$Y(t) = A\sin(2\pi ft + \varphi) \tag{1}$$

where $Y(t)$ is the instantaneous value of the signal at specific time t, A is the amplitude, f is the frequency of the wave, t is time, φ is the phase shift, and 2π is a constant. The waveform generated from the SG is stable and repetitive with clear amplitude, frequency, and phase. The sine wave is split into two waves with the same amplitude, frequency, and initial phase but with a phase difference of 180° (π radians) between them, as shown by the equations below:

$$Y_1(t) = A\sin(2\pi ft + \varphi) \tag{2}$$

$$Y_2(t) = A\sin(2\pi ft + \varphi + \pi) \tag{3}$$

Therefore, the phase-modulated wave in our setup is given by the equation:

$$Y(t) = A\sin(\omega_C t + M_P \sin\omega_m t) \tag{4}$$

where M_p, ω_c, and ω_m are the modulation index, carrier frequency, and modulated velocity, respectively. The carrier signal and the message signal are superimposed to develop the output signal $M_P \sin\omega_m t$, which is a function of $\sin\omega_c t$ and $\sin\omega_m t$. "A" is the amplitude; therefore, the change in phase of the carrier signal is linearly related to the amplitude of the message signal. As shown in Equation (5), the output signal obtained after optical heterodyning at the PD is given by:

$$A\cos(2\pi f_1 t) + A\cos(2\pi f_2 t) = 2A\cos\left(2\pi\left(\frac{f_1 - f_2}{2}\right)t\right)\cos\left(2\pi\left(\frac{f_1 + f_2}{2}\right)t\right) \tag{5}$$

Here, the first term after the equal sign is the frequency difference of the two beat frequencies and gives the output microwave signal. The synchronization of the output signal is dependent on the frequency difference of the input signals f_1 and f_2. The beat frequency from the PD gives the offset frequency f_0, which is the first mode of the generated output frequency. Moreover, the offset frequency can be measured and stabilized, and after undergoing phase modulation, microwave pulses are then generated by applying the SL technique.

As seen in Figure 1(a), the threshold voltage of the temporal waveform of the generated microwave pulse train is selected using the SL formula, $SL = if\ (V < V_{\mathrm{Th}}, 0, 1)$, where V is the applied voltage and V_{Th} is the threshold voltage.

The electronic comparator generates photonic-assisted tunable pulses by comparing two input voltages: the PD voltage (V_{PD}) and the threshold voltage (V_{Th}). In this work, the comparator acts as a voltage threshold detector and switches its output on and off repeatedly, creating a series of pulses in what we call pulse-width modulation (PWM). Figure 1 summarizes the photonic method of generating photonic-assisted tunable pulses using the SL technique.

The duty cycle (D) in microwave pulses is given by the following equation:

$$\mathrm{D} = \frac{T_{on}}{(T_{on} + T_{off})} \times 100\% \tag{6}$$

Consider a periodic pulse wave $y(t)$ with period T. The power is maximum (P_{max}) when the switch is on, and the power is

Figure 1
(a) Sine wave showing the slicing level and (b) tunable pulses showing pulse width (PW) and period (T)

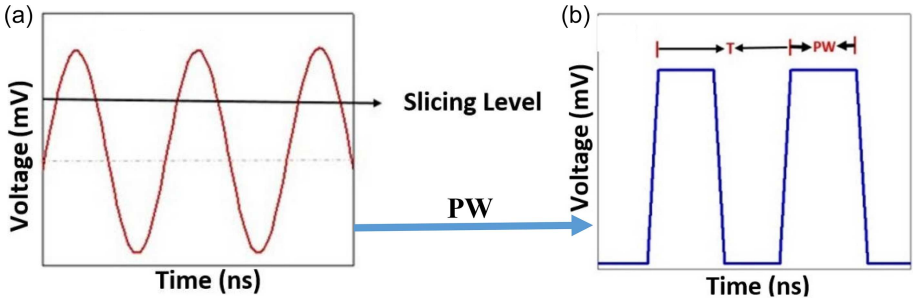

minimum (P_{min}) when the switch is off, with a constant duty cycle D. The average power P_{avg} of the waveform is given by:

$$P_{avg}\frac{1}{T} = \int_0^T y(t)\,\mathrm{dt}, (P_{max} \quad \text{for } 0 < t < \mathrm{D.T} \quad \text{to } \mathrm{P}_{min} \quad \text{for } \mathrm{D.T} < t < T) \tag{7}$$

$$\begin{aligned} \mathrm{P}_{avg} &= \frac{1}{T}\left(\int_0^{DT} P_{max}dt + \int_{DT}^{T} P_{min}\,\mathrm{dt}\right) \\ &= \frac{1}{T}(D.T.\,P_{max} + T(1-D)\,P_{min} \\ &= \mathrm{D}.P_{max} + (1-D)\,P_{min} \end{aligned} \tag{8}$$

As D tends to maximum, $P_{\mathrm{avg}} = \mathrm{D}.\,P_{max}$. Therefore, the average power is directly dependent on the duty cycle. Changing the D causes a phase shift of phase-array antennas depending on the direction required [23]:

$$Phase\,shift(\varphi) = 2\pi(1-D) \tag{9}$$

Each element of the antenna is fed with a microwave signal that is phase-shifted to create diverse electronic delays to form a concentrated beam for a phase array. The number of phase-array antenna elements used determines beamforming array gain aimed at creating thinner beams so as to mitigate path loss between the BS and the UE [24]:

$$G_{array} = 10log_{10}(N) \tag{10}$$

where N is the number of antenna elements.

PWM tunable D shifts into radio frequency phase at the antenna feed system by controlling the time-domain position of the photonic-assisted tunable microwave pulses or by manipulating the on-off switching times of pulses. The relative position of photonic-assisted tunable microwave pulses and duty cycle determines the phase.

3. Experimental Setup

The proposed scheme for generating tunable pulses is shown in Figure 2. Two highly coherent laser sources with wavelengths λ_1 = 1550.349 *nm* and λ_2 = 1550.346 *nm* are used. The wavelength interval between the two optical carriers is 0.003 *nm* (0.375 GHz) at 1550 *nm* transmission window for optical heterodyning, which are combined by the optical coupler and directed to a fully characterized Mach–Zehnder modulator (MZM) where they were modulated. The MZM was characterized, the driving voltage (V_{d}) was set at 5 V, and the biasing voltage (V_{b}) was set at the quadrature point at 7 V according to their Q point characterization measurements. Modulated signals were split into the phase modulator, where phase difference was introduced between the two signals, while the upper arm goes through the PD for optical heterodyning and conversion of optical signals into electrical signals.

In the upper arm, there is an SG for modulating the incoming signals. The phase shifter (PS) changes the phase of the input signal that is mixed with the beat frequency. Optical splitters split the optical signals uniformly, optical combiners combine optical signals from different sources, and the electrical splitters split the electrical signals. Additionally, the electrical spectrum analyzer and the oscilloscope monitor the output signals. Moreover, we have the V_{PD} from the microwave signals and the threshold voltage (V_{Th}) obtained by using the SL formula directed to the comparator, which detects and switches its output on and off repeatedly, creating a series of tunable pulses.

An optoelectronic oscillator set up in Figure 2 combines optical and electrical signals to generate ultra-stable, tunable microwave pulses by comparing the V_{PD} and the threshold voltage using the comparator. This creates a series of pulses with tunable pulse width and period, making it easy to tune the duty cycle, thus achieving phase shift for millimeter-waves (mmWave). The threshold voltage marks the transition point for creating an on-off switch for tunable microwave pulses.

4. Results and Discussion

When the wavelength of two optical sources was set at λ_1 = 1550.349 *nm* and the λ_2 = 1550.346 *nm* and the frequency of the SG varied from 100 kHz to 13.3 MHz, the temporal waveform

Figure 2
Schematic diagram of the photonic-assisted tunable pulse generator

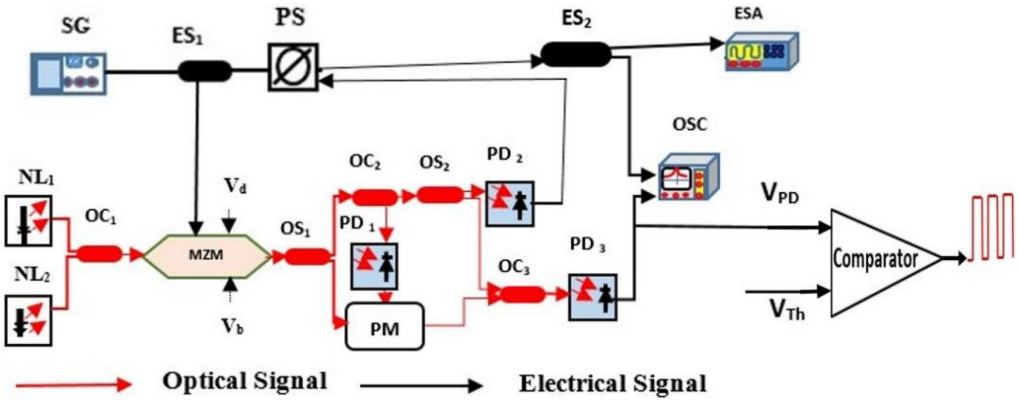

Note: NL: narrow linewidth laser source, OC: optical coupler, ES: electrical splitter, MZM: Mach–Zehnder modulator, V_d: driving voltage, V_b: biasing voltage, PD: photodiode, PM: phase modulator, SG: signal generator, PS: phase shifter, OSC: oscilloscope, ESA: electrical spectrum analyzer, V_{PD}: photodiode voltage, V_{Th}: threshold voltage and comparator.

of the microwave pulse train was generated. By applying the SL technique to the temporal waveform of the generated microwave pulse train, tunable microwave pulses with pulse widths ranging from 0.6 ns to 7.5 μs were generated. This work presents temporal waveforms and tunable pulses using the SL technique.

Figure 3(a) shows the temporal waveform of the generated microwave pulse train of up to 40 μs. By applying a threshold voltage of 8.3 mV to the temporal waveform in Figure 3(a), photonic-assisted tunable microwave pulses with a pulse width ranging from 2.68 μs to 3.46 μs and a period ranging from 4.57 μs to 5.25 μs are generated, as shown in Figure 3(b). The duty cycle of the pulses obtained ranges from 53% to 68%, and the phase shift ranges from 115° to 169°, as shown in Figure 3(c), when the modulating frequency is set at 100 kHz.

When the modulating frequency is set at 186 kHz, a uniformly spaced temporal waveform of the generated microwave pulse train was obtained, as shown in Figure 4(a). By applying a threshold voltage of 7.8 mV to the temporal waveform in Figure 4(a), photonic-assisted tunable microwave pulses with a pulse width ranging from 3.07 μs to 3.32 μs and a period ranging from 5.23 μs to 5.36 μs were generated, as shown in Figure 4(b). The duty cycle of the tunable pulses obtained ranges from 59% to 63%, and the phase shift ranges from 133° to 148°, as shown in Figure 4(c) when the modulating frequency was set at 186 kHz.

Figure 5(a) shows an equally spaced temporal waveform of the generated microwave pulse trains when the modulating frequency was set at 700 kHz. By applying a threshold voltage of 4.42 mV to the microwave waveform in Figure 5(a),

Figure 3

(a) Temporal waveform of the generated microwave pulse train, (b) photonic-assisted tunable pulses, and (c) phase array obtained when the signal generator is set at 100 kHz

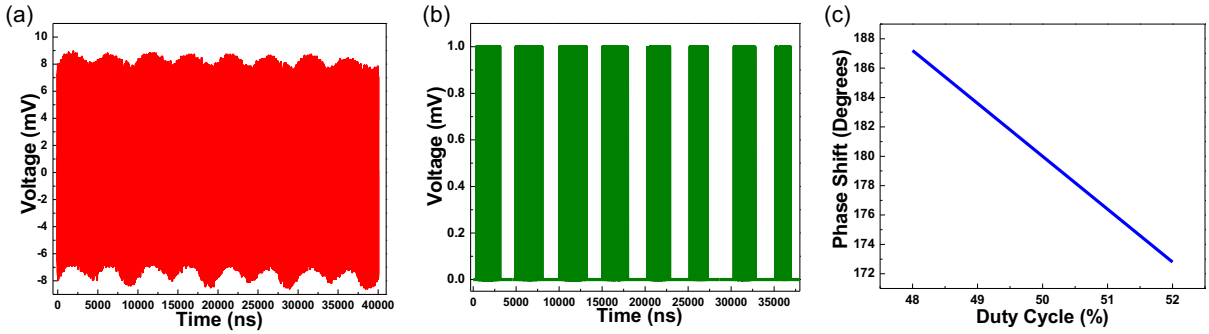

Figure 4

(a) Temporal waveform of the generated microwave pulse train, (b) photonic-assisted tunable pulses, and (c) phase array obtained when the signal generator is set at 186 kHz

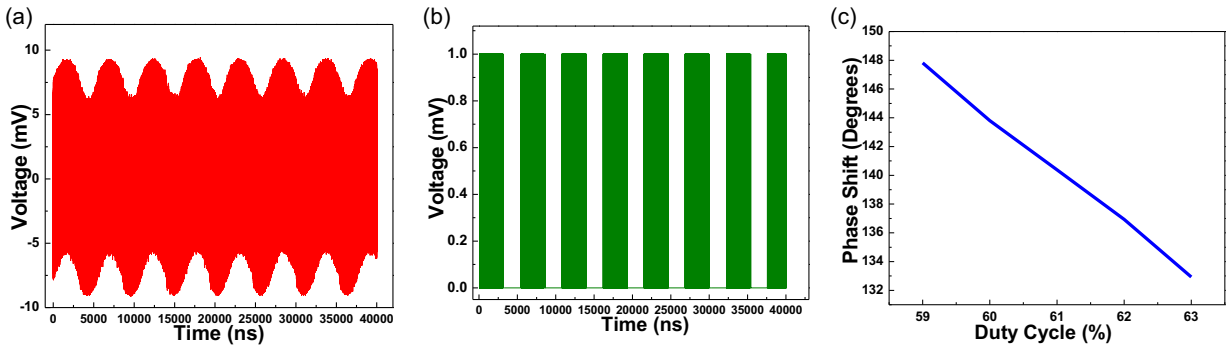

Figure 5

(a) Temporal waveform of the generated microwave pulse train, (b) photonic-assisted tunable pulses, and (c) phase array obtained when the signal generator is set at 700 kHz

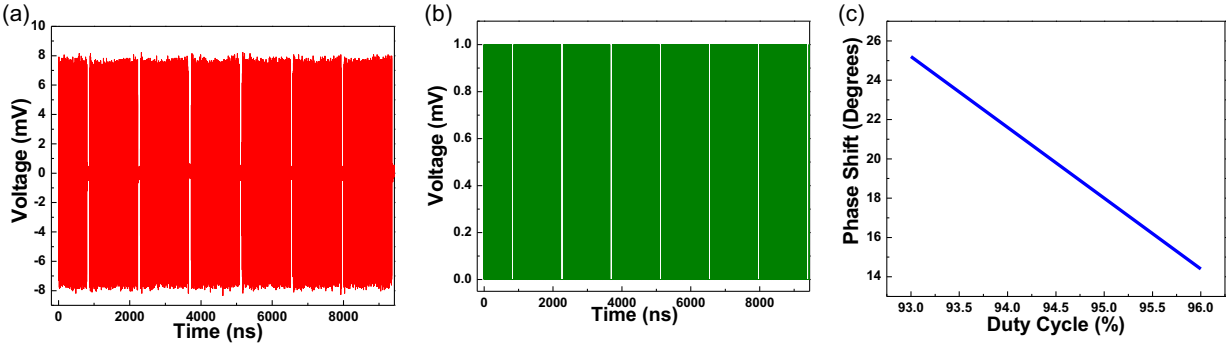

photonic-assisted tunable microwave pulses with an average pulse width of 6.19 μs and an average period of 6.54 μs are generated as shown in Figure 5(b). Tunable microwave pulses generated have a phase shift ranging from 14.4° to 25.2° and duty cycles ranging from 93% to 96%, as shown in Figure 5(c).

By setting the modulation frequency to 1112 kHz, the generated microwave pulse train exhibits a uniform temporal waveform, as shown in Figure 6(a). When the SL technique with a threshold voltage of 0.15 mV is applied to the temporal waveform in Figure 6(a), photonic-assisted tunable microwave pulses with a pulse width ranging from 6.27 μs to 7.45 μs and a period ranging from 7.8 μs to 8.95 μs are generated, as shown in Figure 6(b). The duty cycle of the pulses obtained ranges from 81% to 83%, and the phase shift ranges from 57.6° to 68.4°, as shown in Figure 6(c).

When the modulating frequency is set at 1500 kHz, the temporal waveform of the generated microwave pulse train is generated, as shown in Figure 7(a). By applying a threshold voltage of 4.5 mV to the waveform in Figure 7(a), photonic-assisted tunable microwave pulses with a pulse width ranging from 430 ns to 637 ns and a period ranging from 464 ns to 671 ns are generated, as shown in Figure 7(b). Tunable pulses obtained have a duty cycle ranging from 93% to 96% and a phase shift ranging from 14.4° to 28.8°, as shown in Figure 7(c).

The temporal waveform of the generated microwave pulse train shown in Figure 8(a) was generated when the modulating frequency was set to 1786 kHz. By applying the SL technique at the threshold voltage of 4.57 mV to the temporal waveform in Figure 8(a), tunable pulses with a pulse width ranging from

Figure 6

(a) Temporal waveform of the generated microwave pulse train, (b) photonic-assisted tunable pulses, and (c) phase array obtained when the signal generator is set at 1112 kHz

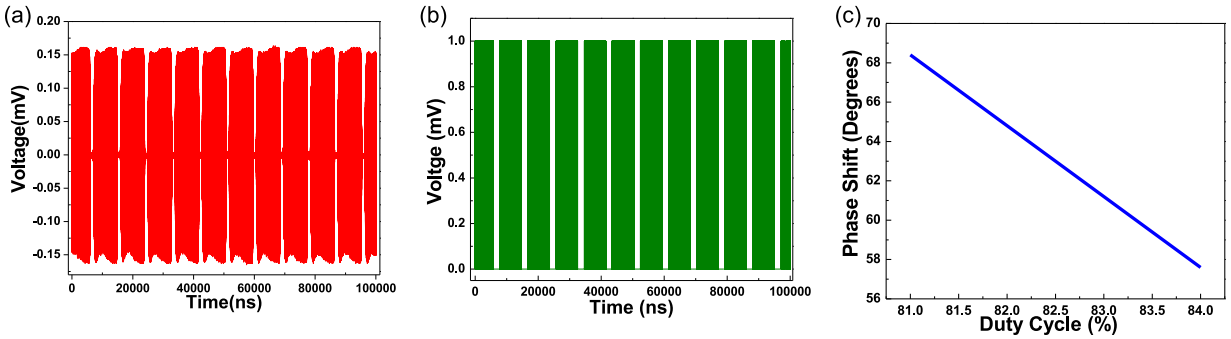

Figure 7

(a) Temporal waveform of the generated microwave pulse train, (b) photonic-assisted tunable pulses, and (c) phase array obtained when the signal generator is set at 1500 kHz

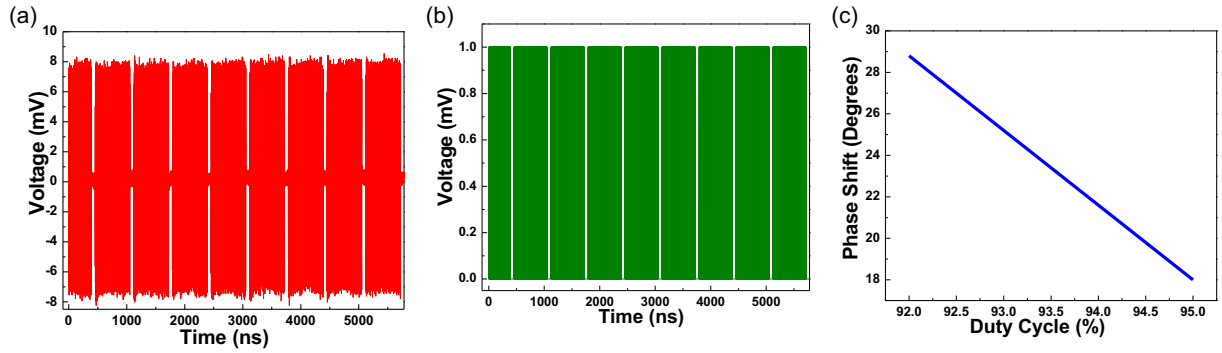

Figure 8

(a) Temporal waveform of the generated microwave pulse train, (b) photonic-assisted tunable pulses, and (c) phase array obtained when the signal generator is set at 1786 kHz

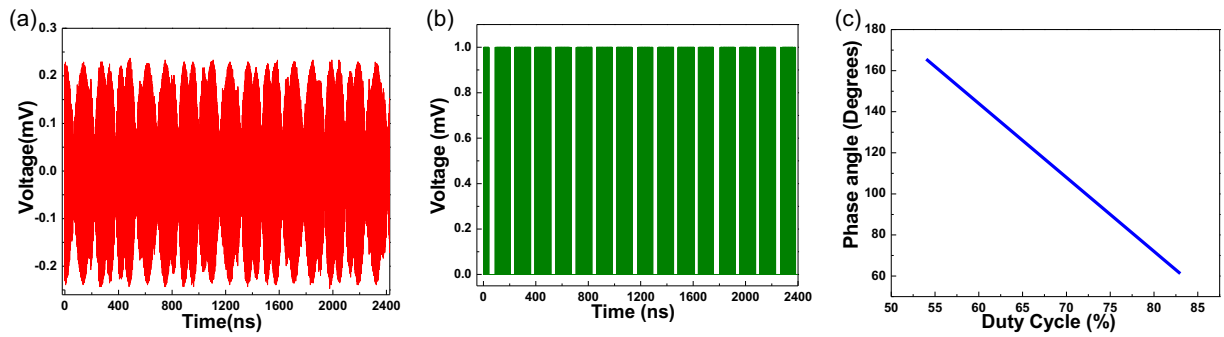

0.05 μs to 0.13 μs and a period ranging from 0.09 μs to 0.16 μs were generated, as shown in Figure 8(b). Microwave pulses generated have a duty cycle ranging from 54% to 83% and phase shift ranging from 61° to 166°, as shown in Figure 8(c).

As shown in Figure 9(a), the temporal waveform of the generated microwave pulse trains follows a uniform pattern. By applying the SL technique to the microwave waveform, microwave pulses with a pulse width ranging from 0.6 ns to 0.64 ns and a period ranging from 1.2 ns to 1.26 ns are generated, as shown in Figure 9(b). Tunable pulses obtained have a duty cycle ranging from 48% to 52% and a phase shift ranging from 172.8° to 187.2°, as shown in Figure 9(c).

When the modulating frequency is set to 13 MHz, a temporal waveform of the generated microwave pulse trains is generated as shown in Figure 10(a). By applying the SL technique at a threshold voltage of 80 mV to the waveform in Figure 10(a), photonic-assisted tunable microwave pulses are generated with a pulse width ranging from 0.7 ns to 0.96 ns and a period ranging from 3.85 ns to 4.15 ns, as shown in Figure 10(b). Tunable microwave pulses generated have a duty cycle ranging from 17% to 23% and a phase shift ranging from 277.2° to 298.8°, as shown in Figure 10(c).

Temporal waveform of the generated microwave pulse train, as shown in Figure 11(a), was generated when the modulating frequency was set at 13.30 MHz. By applying the SL technique at the threshold voltage of 55 mV to the temporal waveform in Figure 11(a), photonic-assisted tunable pulses with a pulse width ranging from 0.6 ns to 1.62 ns and a period ranging from 3.49 ns to 4.15 ns are generated, as shown in Figure 11(b). Microwave pulses generated have a duty cycle ranging from 17% to 42% and a phase shift ranging from 209° to 299°, as shown in Figure 11(c). Phase shift spans from 14° to 299°, depicting strong tunability at higher frequencies, as shown in Table 1, which indicates stronger dependence of pulse properties on modulation

Figure 9

(a) Temporal waveform of the generated microwave pulse train, (b) photonic-assisted tunable pulses, and (c) phase array obtained when the signal generator is set at 10 MHz

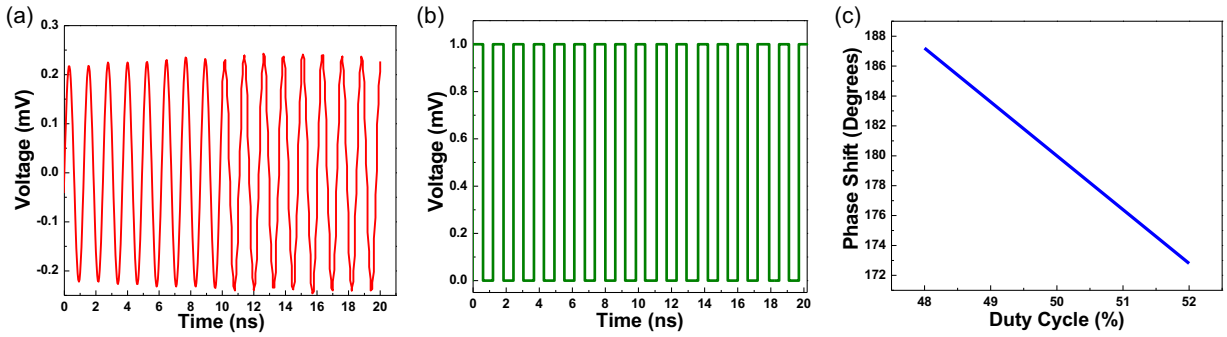

Figure 10

(a) Temporal waveform of the generated microwave pulse train, (b) photonic-assisted tunable pulses, and (c) phase array obtained when the signal generator is set at 13 MHz

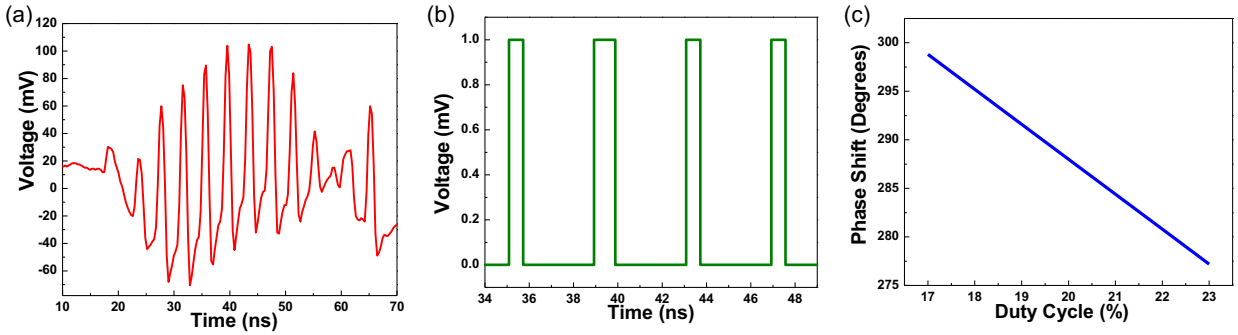

Figure 11

(a) Temporal waveform of the generated microwave pulse train, (b) photonic-assisted tunable pulses, and (c) phase array obtained when the signal generator is set at 13.30 MHz

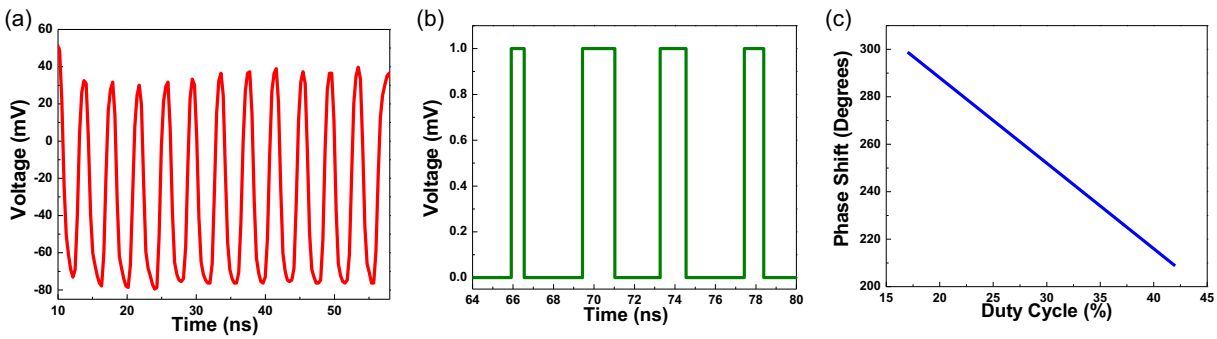

frequency with clear nonlinear and tunable behavior across all measured parameters.

Photonic-assisted tunable microwave pulses generated have a pulse width ranging from 0.6 ns to 7.5 μs with the average duty cycle ranging from 17% to 96%, as shown in Figure 12(a–i), for the respective modulating frequencies ranging from 100 kHz to 13.3 MHz.

From the modulating frequency of 100 kHz to 700 kHz, the phase shift decreases with increasing frequency. The opposite behavior at 1112 kHz and 1786 kHz onward indicates a transition from a capacitive-dominant region to an inductive-dominant region, which eliminates the turn-on losses of the power switches.

Tunability of the microwave pulses generated is exhibited by the adjustable frequencies, tunable period, and tunable pulse width, which is achieved by varying the carrier frequency. The duty cycle of the generated microwave pulses is also tunable. Increasing the duration of the pulses increases the duty cycle; therefore, the duty cycle increases with a decrease in frequency. Finally, the comparison between this work and other published reports is made.

Table 1
Summary of the experimental results corresponding to the photonic-assisted tunable microwave pulses obtained

△λ between two lasers (λ_2–λ_1) nm	Modulating frequency (MHz)	Threshold voltage (mV)	Duty cycle (%)	Phase shift (degrees)
0.003 nm (375MHz)	0.1	8.3	53 ~ 68	115 ~ 169
	0.186	7.8	59 ~ 63	133 ~ 148
	0.7	4.42	81 ~ 84	14 ~ 25
	1.112	0.15	81 ~ 83	58 ~ 68
	1.5	4.5	93 ~ 96	14 ~ 29
	1.786	4.57	54 ~ 83	61 ~ 166
	10	0.05	48 ~ 52	173 ~ 187
	13	80	17 ~ 23	277 ~ 299
	13.3	55	17 ~ 42	209 ~ 299

Figure 12
Duty cycle versus threshold voltage of the photonic-assisted tunable microwave pulses with the modulating frequency ranging from 100 kHz to 13.30 MHz

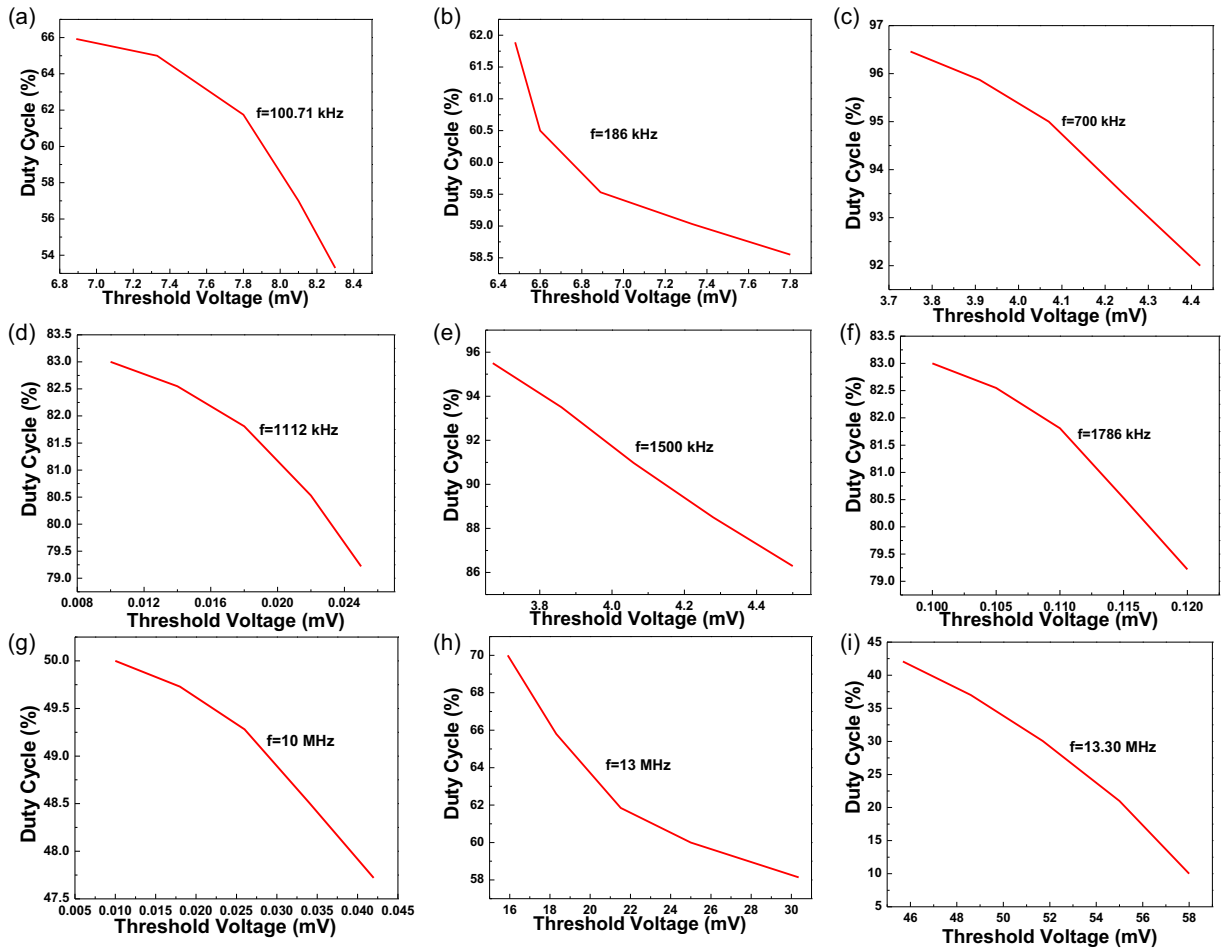

Table 2
Comparison between the reported work and this work

Work	Method	Technique	Wavelength (nm)	Pulse period
Jia et al. [16]	Frequency conversion	Mode-locking	1550	24 ns
Zhang et al. [17]	Optoelectronic oscillator	Mode-locking	1549.892	148.81–297.62 ns
Li et al. [26]	Wavelength Division Multiplexer (WDM)	Mode-locking	1550	481 ps–1.38 ns
Cao et al. [27]	Mach–Zehnder Interferometer (MZI)	Frequency-shifting	1553.3	64–450 ns
Lang et al. [28]	WDM	Mode-locking	1537–1608	549–808 ps
Yang et al. [29]	WDM	Mode-locking	1564.4 nm	0.8–4.3 ps
This work	MZM	Slicing-level technique	1550	1.1–9300 ns

Similar results of pulse widths in the microseconds and nanoseconds range have been reported by Jia et al. [16]. As reported in published work, the period between adjacent pulses can be adjusted [25, 26]. This work records photonic-assisted tunable microwave pulses with tunability of pulse duration between 0.6 ns and 7.5 μs. The comparison between this work and other reported work is shown in Table 2 [27–29].

From Table 2, this work generates microwave pulses with a wide tunability range (1.1–9300 ns), compared to other techniques within the same wavelength transmission window of 1550 nm. This gives a chance to vary the duty cycle and therefore achieve phase shifting, which is a potential candidate for beamforming technology for an antenna array.

5. Conclusion

In this paper, we suggested and demonstrated phase-shifting technique for an antenna array by varying the duty cycle of photonic-assisted tunable microwave pulses experimentally. Tunable microwave pulses with a pulse width ranging from 0.6 ns to 7.5 μs and a duty cycle ranging from 17% to 96% were generated. By adjusting the duty cycle, phase shifts ranging from 14° to 299° were obtained, aimed at beam steering. Phase shift can be used to steer the antennas; the collective effects of phase shifting from multiple antennas create tunable PS for 6G beamforming networks. A concentrated beam of energy creates constructive interference that is aimed at focusing radio energy to a specific UE, thus maximizing spectral efficiency. The phase-array technology demonstrated is a potential candidate for 6G network.

Funding Support

This research was funded by a grant from the African Laser Centre "ALC" (ALC project, Grant Number: HLHA25X TASK NUMBER ALC R016) and Nelson Mandela University Funding (internal fund).

Ethical Statement

This study does not contain any studies with human or animal subjects performed by any of the authors.

Conflicts of Interest

The authors declare that they have no conflicts of interest to this work.

Data Availability Statement

The data that support the findings of this study are available within the manuscript.

Author Contribution Statement

Victor Chepkech Naibei: Conceptualization, Methodology, Formal analysis, Investigation, Data curation, Writing – original draft, Writing – review & editing, Visualization. **Dismas Choge:** Validation, Formal analysis, Resources, Writing – review & editing, Supervision, Project administration. **James Jena:** Methodology, Investigation. **David Waswa:** Conceptualization, Methodology, Validation, Formal analysis, Investigation, Resources, Writing – review & editing, Supervision, Project administration, Funding acquisition. **Duncan Kiboi Boiyo:** Validation, Writing – review & editing.

References

[1] Alwakeel, A. M. (2025). 6G virtualized beamforming: A novel framework for optimizing massive MIMO in 6G networks. *EURASIP Journal on Wireless Communications and Networking*, *2025*(1) 23. https://doi.org/10.1186/s13638-025-02451-2

[2] Li, P., Fan, J., & Wu, J. (2025). Exploring the key technologies and applications of 6G wireless communication network. *iScience*, *28*(5), 112281. https://doi.org/10.1016/j.isci.2025.112281

[3] Vankayala, S. K., Kumar, S., Thirumulanathan, D., Mathur, A., Yoon, S., & Kommineni, I. (2022). Deep-learning based beam selection technique for 6G millimeter wave communication. In *2022 IEEE 33rd Annual International Symposium on Personal, Indoor and Mobile Radio Communications* (pp. 1380–1385). https://doi.org/10.1109/PIMRC54779.2022.9978153

[4] Stepanets, I., & Fokin, G. (2019). Beamforming signal processing performance analysis for massive MIMO systems. In *Internet of Things, Smart Spaces, and Next Generation Networks and Systems: 19th International Conference*, 329–341. https://doi.org/10.1007/978-3-030-30859-9_28

[5] Gkagkas, G., Vergados, D. J., Michalas, A., & Dossis, M. (2024). The advantage of the 5G network for enhancing the Internet of Things and the evolution of the 6G network. *Sensors*, *24*(8), 2455. https://doi.org/10.3390/s24082455

[6] Iyalagha, E. (2025). Beamforming for 5G: A comprehensive analysis and implementation. *International Journal of Advanced Engineering, Management and Science*, *11*(3), 30–36. https://doi.org/10.22161/ijaems.113.6

[7] Enahoro, S., Ekpo, S. C., Chow, K. K., Ji, H., Karimian, N., Uko, M., . . . , & Alabi, S. (2025). Multi-beam beamforming in 5G massive MIMO networks: Normalization techniques and algorithmic performance evaluation. *IEEE Access*, *13*, 191707–191726. https://doi.org/10.1109/ACCESS.2025.3627426

[8] Andras, C. M., Barb, G., & Otesteanu, M. (2025). Comparative analysis of beamforming techniques and beam management in 5G communication systems. *Sensors*, *25*(15), 4619. https://doi.org/10.3390/s25154619

[9] Al-Hatim, Y. M., & Al-Janaby, A. O. (2025). Artificial-intelligent-enhanced adaptive vertical beamforming techniques for 5G networks. *International Journal of Computing and Digital Systems*, *17*(1), 1–18. https://doi.org/10.12785/ijcds/1571024502

[10] Andras, C.-M., Rîcoiu, T.-F., Drugea, D.-A., Barb, G., & Oteşteanu, M. (2024). An overview and classification on beamforming techniques for 5G systems. In *2024 International Symposium on Electronics and Telecommunications* (pp. 1–4). https://doi.org/10.1109/ISETC63109.2024.10797375

[11] Häger, S., Sabbah, B., & Wietfeld, C. (2024). Design aspects for efficient beam training in 6G millimeter-wave networks with mobile users. In *2024 3rd International Conference on 6G Networking*, 173–181. https://doi.org/10.1109/6GNet63182.2024.10765771

[12] Niu, L., Feng, X., Zhang, X., Lu, Y., Wang, Q., Xu, Q., . . . , & Han, J. (2025). Photonic terahertz phased array via selective excitation of nonlinear Pancharatnam-Berry elements. *Nature Communications*, *16*(1), 8159. https://doi.org/10.1038/s41467-025-63127-5

[13] Haque, M. A., Arafat, M. M., Das, I., Alyami, G., Billah, M., Singh, N. S. S., . . . , & Shaman, H. (2025). Predictive modelling and high-performance enhancement smart THz antennas for 6 G applications using regression machine learning approaches. *Scientific Reports*, *15*(1), 34640. https://doi.org/10.1038/s41598-025-18458-0

[14] Zeng, Z., Xu, T., Liu, Y., Lyu, W., Xu, Z., Zhang, L., . . . , & Liu, Y. (2025). Controllable microwave pulse generation in actively mode-locked optoelectronic oscillator based on electro-optic dual-drive Mach-Zehnder modulator. *Optics Express*, *33*(4), 8761–8773. https://doi.org/10.1364/OE.549886

[15] Liu, Y., Ma, Y., Wang, Z., Zeng, Z., Xu, Z., Zhang, L., . . . , & Liu, Y. (2025). Microwave pulse generation with independently tunable pulse width and repetition rate in an actively mode-locked optoelectronic oscillator driven by an amplitude-modulated signal. *Optics Express*, *33*(18), 37381–37393. https://doi.org/10.1364/OE.569926

[16] Jia, X., Tang, L., Liu, S., Ma, H., Tao, T., Chen, L., . . . , & Weng, J. (2021). Frequency-tunable pulsed microwave waveform generation based on unbalanced single-arm interferometer excited by near-infrared femtosecond laser. *Applied Sciences*, *11*(24), 11928. https://doi.org/10.3390/app112411928

[17] Zhang, J., Zhang, D., Zhang, M., Zheng, D., Wang, A., Liu, X., . . . , & Wang, Y. (2022). Tunable microwave pulse generation based on an actively mode-locked optoelectronic oscillator. *Photonics*, *9*(10), 772. https://doi.org/10.3390/photonics9100772

[18] Kumar, S., & Karmbir. (2024). The analogy of switching losses and the importance of switch selection for on-board chargers for electric automobiles. *Gradiva Review Journal*, *10*(6), 502–507. https://doi.org/10.1109/PEDES61459.2024.10961295

[19] Zheng, H., Yang, S., Qiu, Z., Gao, Y., Yang, B., Jin, T., & Chi, H. (2025). Photonic Nyquist folding receiver using optical pulses with discrete pulse position modulation. *Optics Express*, *33*(6), 12699–12708. https://doi.org/10.1364/OE.554156

[20] Hong, S. K., Lathrop, E., Mendez, V. M., & Kim, J. (2015). Ultrashort microwave pulse generation by passive pulse compression in a compact reverberant cavity. *Progress in Electromagnetics Research*, *153*, 113–121. http://dx.doi.org/10.2528/PIER15092406

[21] Wu, Q., Song, Z., Liu, X., Zhang, J., Fang, M., Lu, Q., & Wang, F. (2025). Tunable pulse dynamics in a spun fiber filter-assisted ultrafast laser. *Optics Express*, *33*(19), 39913–39925. https://doi.org/10.1364/OE.572851

[22] Ren, J., Li, P., Ma, C., Xie, Z., Zhao, X., & Zheng, Z. (2025). Generation of random microwave pulse based on random optoelectronic oscillator. *IEEE Photonics Journal*, *17*(2), 5500508. https://doi.org/10.1109/JPHOT.2025.3543866

[23] Heller, M. J., Krismer, F., & Kolar, J. W. (2022). Duty-cycle dependent phase shift modulation of dual three-phase active bridge four-port AC–DC/DC–AC converter eliminating low frequency power pulsations. *IEEE Open Journal of Power Electronics*, *3*, 705–722. https://doi.org/10.1109/OJPEL.2022.3213274

[24] Aljumaily, M., & Abd, H. (2025). Beamforming, handover, and gNB optimization for 5G/6G mmWave in enterprise networks: A ns-3 and NYUSIM-based study. *International Journal of Mechatronics, Robotics, and Artificial Intelligence*, *1*(2), 123–130. https://doi.org/10.33971/ijmrai.1.2.15

[25] Ma, C., Tian, C., Li, S., Xie, Z., Zhao, X., & Zheng, Z. (2024). Tunable microwave pulse generation based on active mode-locked optoelectronic oscillator. *Optics Express*, *32*(20), 35150–35158. https://doi.org/10.1364/OE.535066

[26] Li, W., Dai, L., Huang, Q., Zou, M., Xiao, X., Luo, S., . . . , & Mou, C. (2025). Pulse duration tunable ultra-narrow bandwidth mode-locked lasers. *Advanced Photonics Nexus*, *4*(3), 036016. https://doi.org/10.1117/1.APN.4.3.036016

[27] Cao, R., Wang, G., Li, M., Zhang, J., & Yao, J. (2022). Photonic generation of a microwave waveform with an ultra-long temporal duration using a frequency-shifting dispersive loop. *Optics Express*, *30*(4), 4737–4747. https://doi.org/10.1364/OE.449472

[28] Lang, J., Chen, C., Zhang, P., Qi, M., & Chen, H. (2023). C- and L-Bands wavelength-tunable mode-locked fiber laser. *Photonics*, *10*(12), 1379. https://doi.org/10.3390/photonics10121379

[29] Yang, S., Zheng, J., Qi, Y., Shi, Y., Li, D., Nie, X., & Sun, Z. (2023). Widely-tunable harmonic mode-locked fiber laser by the combination of spectral filtering and gain management. *Optics & Laser Technology*, *157*, 108726. https://doi.org/10.1016/j.optlastec.2022.108726

How to Cite: Naibei, V. C., Choge, D., Jena, J., Waswa, D., & Boiyo, D. K. (2026). Tunable Phase Shifters for 6G Beamforming Networks. *Journal of Optics and Photonics Research*. https://doi.org/10.47852/bonviewJOPR62028031